Author version: *Integrat. Biol., vol.7(2); 2015; 250-262*

In vitro and *in vivo* evaluation of marine sponge skeleton as a bone mimicking biomaterial

Samit K. Nandi[1,**], Biswanath Kundu[2,*], Arnab Mahato[2], Narsinh L. Thakur[3], Siddhartha N., Joardar[4] and Biman B. Mandal[5]

1 Department of Veterinary Surgery and Radiology, West Bengal University of Animal and Fishery Sciences, Kolkata, India

2 Bioceramics and Coating Division, CSIR-Central Glass and Ceramic Research Institute, Kolkata, India

3 CSIR-National Institute of Oceanography, Dona Paula, Goa, India

4 Department of Veterinary Microbiology, West Bengal University of Animal and Fishery Sciences, Kolkata, India

5 Department of Biotechnology, Indian Institute of Technology, Guwahati, India

* 1st Corresponding author; biswa_kundu@rediffmail.com; +91-9831772081

** 2nd Corresponding author; samitnandi1967@gmail.com; +91-9433111065

Abstract: This investigation was carried out to identify and characterize marine sponge as a potential bioscaffold in bone tissue engineering. The marine sponge (*Biemna fortis*) samples were collected from the rocky intertidal region of Anjuna, Goa, India, freeze-dried and converted to pure cristobalite at low temperature. After thorough evaluation of sponge samples by DTA-TGA thermogram, XRD, FTIR, SEM and cell cytotoxicity by MTT assay, bare sponge scaffolds were fabricated by firing at 1190^{o} C. These scaffolds were loaded with growth factors (IGF-1 and BMP-2), checked for quasi-dynamic in vitro release kinetics and finally implanted into femoral bone defects in rabbits for up to 90 days, by keeping empty defect as a control. *In vivo* bone healing process was evaluated and compared using chronological radiology, histology, SEM and fluorochrome labeling studies. SEM revealed that the sponge skeleton possesses a collagenous fibrous network consisting of highly internetworked porosity in the size range of 10-220 μm. XRD and FTIR analysis showed cristobalite phase with acicular and high aspect ratio nature along with increased crystallinity at 725-1190^{o} C. MTT assay demonstrated the non cytotoxicity of the samples. A combination of burst and sustained release profile were noticed for both the growth factors and about 74.3% and 83% total release at day 28. In the radiological, histological, scanning electron microscopy and fluorochrome labeling analysis, IGF-1 impregnated converted sponge scaffold promoted excellent osseous tissue formation followed by BMP-2 loaded and bare one. These observations suggest that the marine sponge alone and in combination with growth factors is a promising biomaterial for bone repair and bone augmentation.

Key words: marine sponge; cristobalite; growth factors; bone healing; biomaterial

1. Introduction

Bone tissue engineering involves the application of cells and/or growth factors in a scaffold template encouraging bone regeneration, which may further stimulate cellular attachment, migration, proliferation and osteoblastic differentiation[1]. In spite of significant breakthroughs in tissue engineering, bone regeneration is still a point of vital importance in diverse clinical setting, such as spinal arthrodesis, prosthetic implants, restoration of maxillofacial structures, pathological bone fractures and non union fractures[2, 3].

Scaffolds are the prerequisites in bone tissue engineering. A wide variety of scaffold matrices are currently used by researchers worldwide for effective bone healing. Selection of these materials largely depends on the tissue properties where it is to be implanted[4]. Ideal characteristics of a bone scaffold material are its suitable biocompatibility, tailorable biodegradability, osteoconductive and osteoinductive nature along with structural mimicking of trabecular bone network[2]. Natural and synthetic scaffolds have been equally used as bone mimicking materials but each has its merits and limitations. Synthetic materials can be developed as per the need, thus matching porosity, microstructure, degradation rate etc. and may be altered as situation demands. In contrast, natural materials are biocompatible and have a better bio-interactive surface for enhanced cellular activity[5]. More specifically, biologically derived materials exhibit optimized structures consisting of extracellular matrix (ECM) that supports cell attachment, migration, proliferation[6] and acts as suitable bioscaffolds in tissue engineering[7, 8].

One such naturally derived material is various exoskeletons of marine sponges, especially demosponges. Apart from their biotechnological applications, marine sponges play an important role in the marine ecosystem. Recent reports show that marine sponges are potential source of therapeutic drugs including molecules for hormone replacement therapy, antibiotic substances, cosmetics etc.[9-13]. The abundance and structural multiplicity of natural marine sponge skeletons including their cell conductive and inductive framework indicate a promising new source of scaffolds for both tissue engineering and tissue regeneration[14-19]. Further, marine sponges exhibit a soft structure of fibrillar, nonfibrillar, and filamentous collagen that systematize the cells into coherent tissues[20, 21]. These collagen fibrils have also been reported for nucleation, formation and growth of apatite crystals from amorphous phase[22]. The presence of complex canal system within sponges helps to generate porous microenvironments which in turn may aid in cellular integration when combined with cells for tissue engineering[23]. Necessity of close proximity to the host bone is its limitation to achieve osteoconduction. Even then, new bone growth is often strictly limited due to its non- osteoinductive nature. To overcome these limitations, a number of growth factors combinations like bone morphogenetic protein-2 (BMP-2)[24] and insulin-like growth factors (IGF-1)[25] have been demonstrated in tissue engineering.

A wide variety of cytokines and growth factors (GFs) have been used from the local bone injury sites to augment bone healing by allowing progenitors and inflammatory cells to migrate. For effective bone regeneration, delivery of these growth factors through a suitable carrier is of utmost importance. Systemic administrations of growth factors are often unpredictable, probably due to their short biological half life, lack of long term stability, and tissue specificity. BMP-2 and IGF-1 are eminent cytokines that plays pertinent role in bone and cartilage formation during embryonic patterning and early skeletal formation[26-29]. For optimum healing, these growth factors should be present at the healing site at a definite concentration. This can be achieved by loading factors in well designed carriers similar to marine porous sponge scaffolds.

Taking these points into consideration, the key objective of the current study was to investigate in vivo bone regeneration capacity of this porous marine sponge (*Biemna fortis*) alone and in combination with growth factors BMP-2 and IGF-1. We hypothesize that loading of these two growth factors within porous sponge scaffolds will lead to slow and sustained release thus influencing sponge performance towards effective in vivo bone regeneration.

2. Materials and Methods

2.1. Fabrication and characterization of porous marine sponge scaffolds

For this study, marine sponge (*Biemna fortis*) samples were collected from the rocky intertidal region of Anjuna, Goa (15° 34' 34.986" N; 73° 44' 23.895" E), India. The Spicule preparations were made with the standard procedure and the identification was carried out with the help of keys presented in the systema porifera vol. 1. The sponge identification was further confirmed by the sponge taxonomist Dr. P.A Thomas from Central Marine Fisheries Institute, India.

The obtained sponge samples were washed thoroughly with deionized water to remove any salt or loosely bound deleterious cations and anions. Post washing, the sponges were freeze dried to obtain a soft fibrous material. To induce porosity, the fibrous material was fired at 725^{o} C first and then naphthalene was used as pore former. In this method, required quantities of naphthalene (<300 μm) and fired sponge were premixed in a dry mixer and compacted by using a cold isostate press at 150 MPa. The compacted cylindrical rods were then dried/ sublimed very slowly upto 60^{o} C to remove naphthalene. The obtained product is a green porous scaffold which was further sintered at 1190^{o} C in a table-top furnace (Vita Vacumat 40T, Germany) at the heating rate of 20^{o} C/ min. The marine sponges were converted to porous scaffold of dimension 5x3 mm dia/height (inset of Fig. 1).

Apparent porosity (AP) and bulk density (BD) were evaluated by water displacement following Archimedes principle. The following formulae were used:

$BD = D/(W-S)$ g/c.c. $AP = (W-D)/(W-S)$ %

where D, W and S are dry, soaked and suspended weight respectively.

Thermal profile of freeze dried fibers were assessed by DTA-TGA (STA 409, Netzsch, Germany) instrument up to 1000^{o} C at a heating rate of 10^{o} C/min in air atmosphere to evaluate conversion/ inversion taking place upto that temperature.

The infrared spectrum of the test samples were analyzed using a FTIR spectrophotometer (Spectrun 100, Perkin Elmer, USA). The spectra had a resolution of 4 cm^{-1} and were recorded in wave number range of 400-4000 cm^{-1}. From the sample data, the background measurements were subtracted. X-ray diffraction was used in order to confirm the conformational transitions occurring and the crystallinity of test samples. X-Ray scans were performed over each sample using Philips X'Pert Pro diffractometer, Netherlands. All scans were performed between 10^{0} to 70^{0} at a speed of 3.0^{0} min^{-1}.

2.2. In vitro cytotoxicity assessment

In vitro cytotoxicity of test sponge materials (5x3 mm) were assessed by MTT method. MC3T3 cell suspension (osteoblast precursor cell line derived from mouse calvaria) in α- MEM growth medium (Gibco, USA) was aliquoted to a 96 well plate containing cell density of 10^{5}/ well. Final growth media volume was made 200 µL/ well. After formation of monolayer following 96 hrs of incubation, the supernatant medium was replaced by fresh growth medium containing test materials (marine sponge). The experimental plates were incubated at 37^{o} C with 5% CO_2 for 24 hours. After incubation period, 20 µL of MTT [3-(4,5-dimethylthiazol-2-yl)-2,5-diphenyl tetrazolium bromide] solution in PBS (5 mg/ mL, Sigma, USA) was added to each well and left for further incubation for 4 h at 37^{o} C. The formazan was quantified by the method of Plumb et al. (1989)[30]. Briefly, the supernatant was removed without disturbing the formazan precipitate and 200 µL of dimethyl sulphoxide (DMSO, Sigma, USA) was added to each well to dissolve the formazan crystals. The contents of the well were mixed thoroughly with micropipette. The final product was read at 595 nm using a plate reader (ECIL, India). All experiments were done in triplicates. Wells without sponge (test material) were controls.

2.3. Fabrication of growth factor impregnated porous scaffolds and its release

Recombinant human bone morphogenetic protein-2 (BMP-2) and recombinant human insulin-like growth factor 1 (IGF-1) were procured from BioVision Research Products, CA, USA (>98% pure). Both vials were centrifuged before opening and reconstituted. Reconstitution was done up to a concentration of 0.1-1.0 mg/mL in ultrapure water (UPW) containing bovine serum albumin (50 µg BSA per 1 µg of protein). Finally, to each sponge test sample (3 samples were taken from each group) of 0.1 cc volume, 30 µg of growth factor was soaked and subjected to brief vacuum followed by freeze drying. Quasi-dynamic in vitro release kinetics was carried out using 1 mL of α-MEM (minimum essential medium) with 1% BSA in a sealed poly-propylene vial. Every 24 hours, fresh medium was replaced and this continued upto 28 days. IGF-1 and BMP-2 release was quantified by using Human IGF-1/ BMP-2 Quantikine ELISA kit (R&D Systems, USA) and the kinetics thus plotted (cumulative) with standard deviations mentioned.

2.4. Animal in vivo experiments

To assess osteogenesis and bone remodeling *in vivo* using a bone defect model in the distal metaphysis of New Zealand white rabbits over a 12 week period, this study was conducted. The study was in compliance with the standards of the Institutions Animal Ethical Committee of the West Bengal University of Animal and Fishery Sciences, India under IAEC Permit No: E. Com. 52 and in accordance with the principles of the Guide for the Care and Use of Laboratory Animals.

Eighteen New Zealand white rabbits of either sex, weighing 1.5-2 kg were randomly distributed into four groups: control group I and the test animals, group II, III and IV. 6 animals were implanted in each group with either pure sponge scaffold (without factors) or IGF-1 and BMP-2 loaded porous sponge. Scaffolds were inserted within the created defects in distal metaphysic region. Prior to surgery, the rabbits were housed in individual cages (temperature/humidity controlled room) with alternating 12-hour cycles of light and dark and given water *ad libitum*.

2.5. Surgical procedure to implant sponge derived scaffold

Under aseptic technique, an incision was made by anaesthesia with injection of xylazine hydrochloride (5 mg/kg) and injection Ketamine hydrochloride (25 mg/kg) body weight intramuscularly. A bone defect ($8\times3\times2.5$ mm^3) in all the animals was performed bilaterally in the distal metaphysis of femur bone with the help of a motorized dental drill. The implants were inserted in the created defects in three test groups keeping contralateral bone empty as control. The wounds were closed in a layered fashion. All the animals were administered injection cefotaxime sodium (Mapra, India) at a dose rate 20 mg/kg body weight intramuscularly, 12 hour interval daily for 5 days and injected meloxicam at 0.2 mL once daily for 5 days. Surgical wounds were inspected daily and wound care was given. All animals were sacrificed after 90 days from start of experiment.

2.6. Radiography and histological assessment

Radiographs of the operative femur were obtained just after implantation and subsequently after every one month interval to assess the status of the implant, host-bone reaction to implant and new bone formation. Radiographs were scored independently by two blinded investigators as per the method of Zhukauskas et al. (2010)[31]. For histological analysis, bone specimens from adjacent side and at the bottom of original bone defect were collected, washed thoroughly with normal saline and was immediately fixed in 10% formalin for 7 days. Subsequently, the bone tissues were decalcified using Goodling and Stewart's fluid (formic acid 15 mL, formalin 5 mL and distilled water 80 mL), followed by fixation with 4% paraformaldehyde. Finally, the samples were embedded into paraffin wax. 4 μm sections were prepared and stained with haematoxyline and eosin to assess the cellular response of host bone to the implants.

2.7. Assessment of newly formed osteoid tissue

Fluorochrome (oxytetracycline dehydrate; Pfizer, India), at a dose of 25 mg/kg body weight was injected intramuscularly for two time points (2-6-2 pattern) before sacrifice for double toning of the newly formed osteoid tissue. Undecalcified ground sections were prepared from the implanted segments of bone and the sections were grounded to 20 μm size using different grades of sand paper. The grounded undecalcified sections were observed under ultraviolet incidental light with an Orthoplan microscope (Excitation filter, BP- 400 range, Leitz, USA).

Oxytetracycline labeled new bone emitted golden yellow florescence when observed under UV light, whereas, matured old bone appeared dark sea green. The animals were euthanized after 90 days and bone samples were collected to study the sponge-bone interface by scanning electron microscopy (SEM). Samples were fixed in 5% glutaraldehyde in PBS buffer for 48 hours followed by gradual ethanol series drying. Dried samples were sputter gold coated before imaging using field emission scanning electron microscope (FESEM, LEO, UK).

3. Results and discussion

Marine sponges due to its availability and biocompatibility may be a potential biomaterial matrix for regenerative medicine. To prove its regenerative potential, we subjected this processed sponges to various tests to assess their physical and chemical properties and ensure compatibility towards various future biomedical related applications.

DTA-TGA thermogram of marine sponge at 1000^{o} C is reported in Fig. 2. The exothermic peak represents the removal of adsorbed water and organic moieties at 345^{o} . Total weight loss of sample was found to be about 18 wt%. A separate sharp exothermic peak at 540^{o} C indicates conversion and formation of new phase. The formed phase was found to be stable upto 1000^{o} C. These findings have been further compared with the XRD spectrum which is represented in Fig. 3a-c.

XRD revealed that the freeze-dried marine sponge is composed of amorphous organic content with very low crystallinity. The sponge powder fired at 725^{o} C had shown appearance of cristobalite phase which subsequently matched with JCPDS PDF No. 76-0936. It is understood that polymorph of silica at normal pressure and temperature converts from α- quartz to β-quartz at 573^{o} C. This form further gets converted to β-tridymite at 870^{o} C and subsequently to cristobalite at a very high temperature of 1470^{o} C. In our present investigation, cristobalite appears at a very low temperature as from Fig. 2 and Fig. 3b. Some varieties of marine sponges are known to absorb silicic acid of sea water and produce monolithic silica spicules by concentric deposition. This internetworked morphology forms a macroscopic structure that supports the sponge above sea water. The siliceous spicules, obtained from this particular marine sponge (*Biemna fortis*) have shown formation of silica specules in the form of cristobalite at very low temperature with very low

crystallite size as in Fig. 3b. When fired at 1190^{o} C, sponge powders had shown reduction of amorphous content and consolidation of crystallinity of cristobalite (Fig. 3c).

FTIR spectra on the other hand shows presence of large carbonate groups at around 1500 cm^{-1} with presence of Si-O-Si groups at around 800 cm^{-1} (Fig. 4a-c). This is an indication of high organic contents in the freeze-dried mass. When the dried mass was fired at 725^{o} C, the carbonate peaks started to be diminishing with appearance of strong Si-O-Si tetrahedra (Fig. 4b). Physically adsorbed –OH groups were also noticed. Similarly, when the powder was fired at 1190^{o} C, carbonate peaks were almost disappeared and there was no degradation of phase of Si-O-Si network which indicates retention of cristobalite phase at 1190^{o} C. Crystallinity was found to increase from 725^{o} C to 1190^{o} C and no other functional groups were noticed from Fig. 4.

MC3T3 cell culture on test samples affected viability of the cells within 24 h. Upon addition of MTT dye in the wells, the metabolic enzymes released from live cells act on MTT to form formazan crystals. Hence, the test materials that were more cytotoxic gave less O.D. values[32].

This was found to be 0.433 ± 0.12 for 725^{o} C fired freeze-dried mass, negative control (cells with no treatment) value being 0.450 ± 0.9. Confluent monolayer of culture of MC3T3 and formation of formazan crystals after adding MTT are given in Fig. 5.

Fig. 6 shows the microstructure of the powders when the freeze dried mass was fired at 725^{o} C. Acicular rods of cristobalite having a very high aspect ratio were noticed throughout the microstructure with a typical diameter of 5-10 μm. Individual needles were also found to be sintered at the location of the junctions. Powdered sample sintered at 1190^{o} C showed a highly inter-networked porosity in the size range of 10-220 μm (Figs. 7a and b). Acicular nature of the cristobalite were also noticed which was primarily found to be sintered at the periphery. The temperature of 1190^{o} C was selected so that pore closer could be avoided when fired at even higher temperature. Apparent porosity A.P. and B.D. of the samples were found to be about 52% and 1.1 g/cc respectively. Porosity in this range along with micro to macro pore size range is desirable for tissue and cell ingrowth. These porous scaffolds have been used subsequently for incorporation of different protein growth factors and subsequent effect of these scaffolds on bone tissue development.

3.1. In vitro GF release profile

Fig. 8 shows the in vitro GF (IGF-1 and BMP-2) release kinetics both individual (with standard deviation) and cumulatively (inset) on a day-to-day basis upto 28 days in presence of α-MEM. It was found that there was about 21.8% and 27.2% GF release at day 1 for IGF-1 and BMP-2 respectively. Almost 52.6% and 77% GF were released at day 7 for IGF-1 and BMP-2 respectively. After the initial burst release, both the GFs showed almost sustained kinetics of release upto 28 days. At day 28, about 74.3% and 83% of total loaded IGF-1 and BMP-2 were released respectively. The most plausible reason for more sustained manner release of IGF-1 after day 3 in α-MEM may be due to the fact that IGF-1 consists of 70 amino acids in a

single chain with three intramolecular disulfide bridges, also having a mol. wt. of 7.6 kD while BMP-2 has two 114 amino acid residue subunits, with a calculated molecular mass of ~ 26 kDa. Converted marine sponge was composed of cristobalite which was adsorbed more in case of IGF-1 than BMP-2 due to these different protein crystal structures. However, further experimentation is needed to conclude on this.

3.2. SEM of in vivo samples

After three months the defect site was compared for 1190^{o} C bare porous scaffolds along with IGF and BMP loaded scaffold which was further compared without any implant at the defect site. Defect site without any implant shows formation of soft tissues only with collagen fibrils interconnected throughout the defect site after 3 months (Figs. 9a and b). There is no formation of hard tissues even after this period and the defect site gap remained open. Absence of any RBC was indicative of less chance of recurrence of infection. Sporadic granular tissue was also noticed which indicates that the soft bone formation is yet to be completed.

Bare scaffold (without any growth factor loading) in the defect site on the other hand showed invasion of bone tissues throughout the matrix of porous scaffold where individual needle shaped rods could be seen (Figs. 9c and d). Matured osteoblastic cell which is an indicative of hard tissue formation was in close approximation on the periphery of the implant however interfacial gap was found to be present between the implant and matured bone. Most probably, bare porous scaffold acted as a bioactive catalyst on the periphery and its subsequent maturation. Interfacial gap was found to be 1-5 μm. Collagens network was noticed from the periphery of the scaffold to the matured bone surface. Few needle shaped fibers was also started degrading but deposition of calcium-phosphate crystals could not be noticed.

IGF (Figs. 9e and f) and BMP (Figs. 9g and h) loaded porous scaffold showed much enhanced bone formation in contact with the implant at the defect site. BMP loaded scaffold showed better bone approximation than the IGF one. Interfacial gap was found to be diminished for both the cases. Mature osteoblastic cells were found throughout the scaffold when loaded with IGF and BMP. Pores of the implants were also found to be closed when in contact with cortical bone adjacent to the implant. Superior matured bone deposition was noticed in case of BMP. It was due to the presence of IGF and BMP which promoted superior dissolution of porous scaffold than the bare one. Fibrous collagen was found to be more in quantity in case of IGF than BMP which is an indication that further time is required for maturation of soft bone tissues. There were no granular tissues for both these type of implant.

3.3. Histological study

Control sample (without any implant) showed (Fig. 10a) a moderate architecture of compact bone characterized by formation of osteon and few haversion canals. In cellular activity, osteoclasts are prominent at the margin of the cortical region. Few blood vessels corroded the newly formed bony structure along with invasion of osteoclast indicating remodelling of bones. Bare sponge scaffold bone section depicted (Fig. 10b) a well formed osteon embedded in matrix characterized by congestion, calcification of

some newly formed osteons with osteoblastic and osteoclastic activities. The medullary cavity showed well organized adipose tissues along with mononuclear cells, few megakaryocytes and RBC. IGF-1 loaded sponge scaffold bone sample showed (Fig. 10c) numerous haversian canals interspissated with few bony specules. Medullary cavity showed moderate amount of RBC, mononuclear cells and one solitary megakaryocyte. The architecture details are well formed containing angio- invasion, calcification and remodelling of bones. Finally, BMP-2 loaded sponge scaffold bone sample showed (Fig. 10d) moderate amount of bony structure along with periarticular chondrocytes. The solid compact bone showed congestion, mononuclear cell infiltration, formation of new osteons along with lacunae. The haversian canal is constricted in some places due to formation of newly formed vessels for facilitating remodelling and orientation of new bone. Cellular structure of osteoblast is numerous. Table 1 shows a score sheet prepared for different cellular events (fibro-vascular proliferation, infiltration with mononuclear cells, osteoclastic/ osteoblastic activity, mucin deposit and vascularity) at 3 months after observing the histological images for all group of animals. Statistical significance was also carried out for particular 2 groups of animals and represented in the table.

3.4. Fluorochrome labeling study

At three month time point in control sample (without implant), the process of new bone formation was moderate from both the ends (Fig. 11a). The intensity of newly formed bony tissues was more in central zone as compared to peripheral area. The defect was moderately filled with newly formed osseous tissue as evidenced by presence of golden yellow fluorescence. Union in the defect site of bone was under process. In bare scaffold implanted bone showed (Fig. 11b) presence of more golden yellow fluorescence in central zone signifying newly formed osseous tissue in endosteal side as compared to control sample. The sea green appearance at the outer border of central zone indicated existence of old bone in periosteal side. In IGF-1 loaded scaffold sample demonstrated (Fig. 11c) presence of golden yellow fluorescence both in central and peripheral zone i.e., endosteal as well as in periosteal side indicating more new bone formation. Similarly, in BMP-2 loaded sponge sample showed (Fig. 11d) wide coverage of golden yellow fluorescence in endosteal side vis-à-vis its presence in periosteal side although intensity was more in central zone.

3.5. Radiological study

Fig. 12a (0, 1, 2, 3) shows the radiographs for control (no implant) samples after day ‘0’ and 1-3 month respectively. On ‘0’ day, radiographs showed the cortical defect in distal femur devoid of any implant resulting to radiolucent gap. The defect was of similar shape and size to that of animals of other groups. On day 30, radiographs revealed with minimal periosteal reaction and smoothing edges of cortical bone defect. The size of oval shaped defect has been reduced than earlier days suggesting initiation of bone healing. On day 60, radiographs showed that there was considerable reduction in the defect size which was in the course of obliteration by osseous tissue material of similar density to that of host bone. On day 90, radiographs

showed that the defect was not fully obliterated by newly grown bony tissue as evidenced by radiolucent shadow of defect. However, more amount of hard tissue material was grown as compared to earlier days.

Similarly, for bare porous scaffold sample (Fig. 12b, 0-3), on day '0', the bone defect treated in distal epiphysis of femur showed presence of radiodense scaffold in the cylindrical shaped defect. The material has been observed as denser than the bone without any involvement in the adjacent soft tissue. On day 30, density of the filling material appeared to be unaltered or slightly reduced even without any periosteal or soft tissue reaction. Subsequently, on day 60 in the distal epiphysis, the shape has been changed from cylindrical to oval. The periphery of the filling material showed reducing the size indicative of onset of replacement of sponge material by newly grown bony tissue. The radiograph on day 90 showed presence of minute amount of material with initiation of radiolucency indicative of ignition of resorption vis-à- vis bridging of the gap with presence of faint osseous tissue.

Fig. 12c, 0-3 show radiographs of IGF-1 loaded porous scaffold material after day '0' and 1-3 month respectively. In this group, on day '0', implant was evidenced as radiodense material in the distal epiphysis of femur. On day 30 and 60, there was presence of the faint shadow of the implant material which was indicative of appreciable process of implant 'take up' by the host tissue. On day 90, the radiograph showed reduction of the defect size with decrease radiodensity than earlier days and with increased radiolucency indicating the process of resorption of the material and simultaneously formation of newly grown bony tissue within the defect. The 'taking up' of the implant with the host tissue happened in more efficient way.

Radiographs of BMP-2 loaded porous scaffold material (Fig. 12d, 0-3) showed the bony defect filled with implant in distal epiphysis of femur with well circumscribed radiodense material. The radiological features on 30th day revealed less radiodensity of the material than that of day '0'. The day '60' radiograph of the same group showed faint shadow of material with moderately increased radiolucency in defect area indicating evidence for onset of resorption of implant material. On day 90, the process of resorption was more than that of 60th day as evidenced by increased radiolucency in the defect area. Moreover, from the score sheet, an attempt has been made to measure the semi-quantitative bone formation in all the groups at each time point of radiology which has been presented in Table 2.

Identification of suitable natural bioscaffolds as bone regeneration capabilities as well as local delivery system of growth factors in bone defect site is a major research thrust area. A natural marine sponge skeleton possess hydration potential of the fiber, open interconnected channels formed by the fiber network, the collagenous composition of the fiber, and the structural diversity of fiber architecture[14]. Marine sponges are able to stimulate osteoblast attachment, proliferation, migration and differentiation *in vitro* with void dimensions ranging 500-1250 μm signifying its tremendous role as a bioscaffold for bone tissue engineering[6]. Development of new tissue in a scaffold is markedly dependent by the composition, porosity and three-dimensional structure of the scaffold onto which cells are cultured[33, 34]. Porosity inside the marine sponge body is generated by a system of pores (ostia), channels and chambers providing nutrition to the

living sponge and gas exchange from the surrounding water. Porosity in any scaffold is the prerequisite for maximal invasion of osteoblastic cells for effective bone regeneration[35]. Moreover, optimum pore dimension with interconnected porosity of the scaffold is also vital for cellular infiltration and osteoblast amalgamation into bone tissue which should be in between 100-250 μm[36, 37]. Besides, pore dimension is directly linked with mineralized bone formation[38]. In this study, highly internetworked porosity with a pore dimension range of 10-220 μm was used having similarity to the pore size in human compact bone[39].

Mesh-like arrangement of collagen fibres within the sponge skeleton is microstructurally alike to the lattice structure of fibres in human trabecular bone enabling attachment, migration and proliferation of osteoblasts[39, 40]. Further, chemotactic properties of collagen provide a natural environment for cellular attachment and aggregation making it suitable as tissue engineering scaffolds[18, 41].Although marine sponge has many qualities as tissue engineering scaffold, it has no direct osteoinductive property in orthopedic bone healing[18].

This can be achieved by addition of growth factors which in turn helps in bone formation when compared to use marine sponge alone. In this study, we report a simple processing technique of natural marine sponge preparation and characterization along with in depth *in vitro* study in cell line and *in vivo* biological responses in animal model alone and in combination with growth factors like BMP-2 and IGF-1.

In the present investigation cristobalite appears at a very low temperature after thermal conversion of freeze-dried *Biemna fortis* sponge. In the present work, this particular marine sponge has shown formation of silica specules in the form of cristobalite with very low crystallite size. FTIR spectra on the other hand shows presence of large carbonate groups at around 1500 cm^{-1} with presence of Si-O-Si groups at around 800 cm^{-1}. This is an indication of presence of mainly organic contents in the freeze-dried mass. When the freeze-dried mass was fired at 725^{o} C, the carbonate peaks were started to be diminished with appearance of strong Si-O-Si tetrahedra. Physically adsorbed –OH groups were also noticed. When the powders were fired at 1190^{o} C, carbonates were almost disappeared and there was no degradation of phase of Si-O-Si network which indicates the cristobalite phase was retained even after firing at 1190^{o} C. However crystallinity was increased from 725^{o} C to 1190^{o} C.

MTT assay using MC3T3 preosteoblastic cells showed very similar OD values of sample (725^{o} C fired freeze dried sponge) with that of negative control which was indicative that the sample was completely non-cytotoxic and biocompatible with bone forming cells. Fubini et al.[42] showed that cristobalite in dust form when fired at very high temperature (1300^{o} C) showed cytotoxicity on a particular cell line which is not the case in the present investigation. Cristobalite obtained from marine sponge were converted at low temperature and when fired at 1190^{o} C, just retained its structure with higher crystallinity and since it was implanted in a porous scaffold form, there was no adverse effect on bone cells lines. So, in this work we have shown for the first time that this particular category of marine sponge can be a great natural source of

biocompatible cristoballite with acicular and high aspect ratio nature. Quasi- dynamic in vitro GF release profile from converted sponge scaffold showed that IGF-1 and BMP-2 were very much comparable with respect to its kinetics although IGF-1 retained slightly better GF adsorption even after 28 days. Both the GF showed comparable sustained release profile. FDA approved BMP-2 is a GF which plays a crucial role for expression of osteogenic markers and help induce osteogenesis while IGF-1 stimulate osteoblast growth and proliferation which in turn promotes osseo-integration at local site[43]. This in vitro GF release profile thus found to be very promising before tried in animal subject.

Radiological investigation, a noninvasive technique is one of the important *in vivo* characterization methods to assess union at the host bone-material interface during the post- operative follow up[44] and to evaluate the nature and dynamics of new bone formation and osseointegration of a biomaterial[45]. A distinct radiodensity of the material is observed immediately after implantation in bone defect and the gradual reduction of this density of is considered to be an indication of in-growth of osseous tissue from the host bone towards the implant vis-à-vis initiation of bone healing[46]. In the present study, bare sponge sample showed distinct radiodensity immediately after implantation which however, remained unaltered upto 60 days. The periphery of the filling material showed reduced size indicative of onset of replacement of sponge material by newly grown bony tissue. The radiograph on 90 days of same group showed presence of minute amount of material with initiation of radiolucency indicative of initiation of resorption vis-à-vis bridging of the gap with presence of faint osseous tissue. In IGF-1 loaded sponge material, the radiodensity of the material is considerably reduced on 60 days and present as a faint shadow indicating appreciable process of implant "take up" by the host tissue. On "90" days, the radiograph showed reduction of the defect size with decrease radiodensity than earlier days and with increased radiolucency indicating the initiation of resorption of the material and simultaneously formation of newly grown bony tissue within the defect. The "taking up" of the implant with the host tissue happened in more efficient way. The bony defect filled with the BMP-2 loaded sponge sample showed gradual diminishing of radiodensity of material with moderately increased radiolucency in defect area indicating evidence for onset of resorption of implant material. On "90" days the process of resorption was more than that of "60" days as evidenced by increased radiolucency in the defect area. Significant in-growth of new bone formation with growth factor loaded implant could be expected than bare implant[47]. Due to greater hydration potential, it is expected that marine sponge skeleton can absorb and release recombinant BMP-2 and IGF-1 and induce expression of alkaline phosphatase and thus in turn promote bone cell differentiation and osteogenesis[18]. In the present study, the radiological score sheet provide us an indication of bone formation based on different animal response. Though it is not an exact quantitative analysis, an attempt has been made to explain the bone formation activity in semi quantifiable basis.

In the present study, fluorochrome labeling especially with tetracycline markers also confirmed the bone regeneration capability in the implanted area[46]. Tetracycline molecule generally pursues and absorbs in

places where active mineralization tissue takes place[48]. It has fluorescence property in ultraviolet light which produces bright golden yellow and dark- sea green fluorescence giving an indication of new bone and old bone respectively[49]. In the present study, the bare sponge implanted bone showed presence of enhanced golden yellow fluorescence in central zone signifying newly formed osseous tissue in endosteal side as compared to control sample. In IGF-1 loaded sponge sample demonstrated presence of higher golden yellow fluorescence both in central and peripheral zone, i.e. endosteal as well as in periosteal side indicating more new bone formation. Similarly, in BMP-2 loaded sponge sample showed a wide coverage of golden yellow fluorescence in endosteal side vis-à-vis its presence in periosteal side although intensity was more in central zone. Presence of higher golden yellow fluorescence in IGF-1 and BMP-2 loaded sponge samples may be due to the direct effects of growth factors which in turn help in cellular proliferation, osteoblastic activity and eventual more new bone formation. In control samples, rate of new formation is less distinct as observed by homogenous, non-fluorescent area although the process of new bone formation was active in the defect site.

Histologically IGF-1 loaded sponge scaffold bone sample showed numerous haversian canals, osteoblastic activity along with angioinvasion, calcification and remodelling of bones. The BMP-2 loaded sponge scaffold bone sample showed moderate amount of bony structure with numerous osteoblast and constricted haversian canal in some places due to formation of newly formed vessels for facilitating remodelling and orientation of new bone. Higher osteoblastic activity in both the cases may be due to direct effect of these growth factors which help in cell proliferation and cytodifferentiation[50]. Bare sponge scaffold impregnated bone section depicted a well formed osteon embedded in matrix characterized by congestion, calcification of some newly formed osteons with osteoblastic and osteoclastic activities. The observation of regenerated bone grown in direct contact with the bare sponge scaffold, even in the absence of BMP-2 and IGF-1, suggests it is also osteoconductive and highly compatible for bone regeneration. In control sample (without any implant) showed a moderate architecture of compact bone characterized by formation of osteon and few haversion canals. Fibrovascular proliferation was statistically significant or statistically different for scaffolds loaded with IGF-1 than converted sponge scaffold ($p \leq 0.05$) while parameters like vascularity and osteoblastic activity were found to be statistically significant for both IGF-1 and BMP-2 loaded scaffolds than the control (cf. Table 1). However, osteoclastic activity was also found be statistically significant for both IGF-1 and BMP-2 loaded scaffolds than the control. This indicates that both osteoclastic and osteoblastic activity were taking place simultaneously while bone healing, but, IGF-1 and BMP-2 actually helped for osseo-integration which was indicated by better fibro-vascular proliferation and vascularity than control or converted sponge bare scaffold alone.

Morphological evaluation at the bone-implant interface by SEM after three months, the defect site was compared bare porous scaffolds along with IGF and BMP loaded scaffold which was further compared without any implant at the defect site. Defect site without any implant shows formation of soft tissues only with collagen fibrils interconnected throughout the defect site. There is no formation of hard tissues even

after this period and the defect site gap remained open which indicates that the soft bone formation is yet to be completed. In bare scaffold (without any growth factor loading) in the defect site on the other hand showed invasion of bone tissues throughout the matrix of porous scaffold where individual needle shaped rods could be seen. Matured osteoblastic cell which is an indicative of hard tissue formation was in close approximation on the periphery of the implant however interfacial gap was found to be present between the implant and matured bone. Bare porous scaffold may have acted as a bioactive catalyst on the periphery and its subsequent maturation. Collagens network was noticed from the periphery of the scaffold to the matured bone surface. IGF-1 and BMP-2 loaded porous scaffold showed much enhanced bone formation in contact with the implant at the defect site. BMP loaded scaffold showed better bone approximation than the IGF one. Interfacial gap was found to be diminished for both the cases. Mature osteoblastic cells were found throughout the scaffold when loaded with IGF and BMP. Pores of the implants were also found to be closed when in contact with cortical bone adjacent to the implant. Superior matured bone apposition was noticed in case of BMP. It was due to the presence of IGF and BMP which promoted superior dissolution of porous scaffold than the bare one. Fibrous collagen was found to be greater in quantity in case of IGF than BMP which is an indication that further time is required for maturation of soft bone tissues. In the present study, interfacial gap was least as compared to bare scaffold which might be due to new invasions of osteoblastic cells in the implant material as a result of sustained release of growth factors like IGF-1 and BMP-2[51]. In vitro burst release of BMP-2 from other scaffolding materials was noticed intended for healing of femur segmental defect[52].

The fundamental nature of the bone-tissue engineering archetype involves combining approach of soluble osteogenic molecular signals with diverse insoluble signals or substrate and thus developing 3D scaffolds for the initiation of *de novo* tissue induction and morphogenesis[53-58]. Osteogenic soluble molecular signals of the transforming growth factor-β (TGF-β) superfamily are of paramount necessity for bone formation by induction[55, 59]. The release of BMP-2 and IGF-1 must be localized to the defect site as well as regulated for effective and enhance bone regeneration[60, 61]. The ideal release approach for BMP-2 and IGF-1 in large critical-sized defects that cannot heal spontaneously is a burst release that recruits osteoprogenitor cells into the scaffold, followed by a sustained release that promotes osteoblastic differentiation[37, 62]. Nevertheless, ideal delivery system is generally accepted, different release strategies have been compared systematically, especially in more difficult bone defects[37, 60]. In the present study, the combined burst and sustained release achieved with the sponge + BMP-2 and sponge + IGF-1 scaffolds was more effective than the bare marine sponge, thereby suggesting this scaffold is a more efficient delivery system. In another in vivo study, the release of BMP-2 from the collagen sponge has been reported to be more sustained, demonstrating a burst release followed by a sustained release until day 14[37,63]. The availability of BMP-2 at later time points enhances bone regeneration due to recruitment of additional osteoprogenitor cells at the fracture site[64-66].

4. Conclusion

This study examined the influence of IGF-1 and BMP-2 impregnated marine sponge scaffolds on in vivo performance over the course of 90 days. We have demonstrated that this particular category of marine sponge can be a great natural source of non-cytotoxic and biocompatible cristoballite with acicular and high aspect ratio nature. Quasi-dynamic in vitro GF release profile from converted sponge scaffold showed that IGF-1 and BMP-2 were very much comparable with respect to its kinetics although IGF-1 retained slightly better GF adsorption even after 28 days. In vivo characterizations (SEM, histology, radiology and fluorochrome labeling), our results suggest that growth factor loaded sponge skeleton can reduce the time of early bone formation and implant infiltration when compared to the bare coral scaffolds. As a whole, this study signifies that the marine sponge skeleton is a new source of natural bioscaffold for the repair of bone defects. The pore size, microstructure, interconnected pore network, permeability, and composition of the sea sponge skeleton emerge to aid in successful osteoblastic cellular attachment. The presence of osteoinductive and conductive frameworks together with the abundance and structural multiplicity of natural marine sponge skeletons signifies its role as a new source of scaffold for bone regeneration as well as local delivery vehicles of growth factors for bone healing.

Acknowledgements

The authors wish to express their sincere thanks for the financial support by the Department of Biotechnology, Ministry of Science and Technology, Government of India as a part of National Bioscience Award-2008 for career Development [BT/HRd/34/15/2008]. We wish to thank the Director CSIR-Central Glass and Ceramic Research Institute, Kolkata, India, Director CSIR-NIO, Goa, India and Vice Chancellor, West Bengal University of Animal and Fishery Sciences, Kolkata, India for their generous and kind support to this work. All the personnel involved in the characterization of the materials are sincerely acknowledged. CSIR-NIO contribution No. is……(#).

Reference

1. S. Bose, M. Roy and A. Bandyopadhyay, Trends in Biotechnology, 2012, 30, 546-554.
2. S. P. Bruder and B. S. Fox, Clin Orthop Relat Res, 1999, 367, S68-S83.
3. S. A. Gittens and H. Uludag, J Drug Target, 2001, 9, 407-429.
4. A. Vats, N. S. Tolley, J. M. Polak and J. E. Gough, Clin Otolaryngol Allied Sci, 2003, 28, 165-172.
5. B. Sharma and J. H. Elisseeff, Ann Biomed Eng, 2004, 32, 148-159.
6. D. Green, D. Walsh, S. Mann and R. O. C. Oreffo, Bone, 2002, 30, 810-815.
7. S. Badylak, A. Liang, R. Record, R. Tullius and J. Hodde, Biomaterials, 1999, 20, 2257-2263.
8. K. J. L. Burg, C. R. Culberson, K. G. Greene, A. B. Loebsack, W. R. Roland, W. D. Holder Jr, C. R. Halberstadt and R. J. Beiler, Crit Rev Biomed Eng, 2000, 28, 383-387.
9. H. Ehrlich, Biological materials of marine origin, Springer, 2010.
10. N. L. Thakur and W. E. G. Muller, Curr Sci, 2004, 86, 1506-1512.

11. X. Wang, H. C. Schroder, V. Grebenjuk, B. Diehl-Seifert, V. Mailander, R. Steffen, U. Schlobmacher and W. E. G. Muller, Marine drugs, 2014, 12, 1131-1147.

12. E. Cunningham, N. Dunne, G. Walker, C. Maggs, R. Wilcox and F. Buchanan, J Mater Sci: Mater Med, 2010, 21, 2255-2261.

13. M. Nicklas, W. Schatton, S. Heinemann, T. Hanke and J. Kreuter, Drug Develop Indus Pharma, 2009, 35, 1035-1042.

14. H. Ehrlich, in Biomimetic Biomaterials: Structure and Applications, ed. A. J. Ruys, Woodhead Publishing, Cambridge, 2013, pp. 47-67.

15. H. Ehrlich, E. Steck, M. Ilan, M. Maldonado, G. Muricy, G. Bavestrello, Z. Kljajic, J. L. Carballo, S. Schiaparelli, A. Ereskovsky, P. Schupp, R. Born, H. Worch, V. V. Bazhenov, D. Kurek, V. Varlamow, D. Vyalikh, K. Kummer, V. V. Sivkov, S. L. Molodtsov, H. Meissner, G. Richter, S. Hunoldt, M. Kammer, S. Paasch, V. Krasokhin, G. Patzke, E. Brunner and W. Richter, International Journal of Biological Macromolecules, 2010, 47, 141-145.

16. E. Steck, M. Burkhardt, H. Ehrlich and W. Richter, Xenotransplantation, 2010, 17, 153-159.

17. H. Ehrlich and H. Worch, in Porifera Research: Biodiversity, Innovation and Sustainability, ed. E. Hajdu, Série Livros 28. Museu Nacional, Rio de Janeiro, 2007, pp. 217-223.

18. D. Green, D. Howard, X. Yang, M. Kelly and R. O. C. Oreffo, Tissue Eng, 2003, 9, 1159-1166.

19. Z. Lin, K. L. Solomon, X. Zhang, N. J. Pavlos, T. Abel, C. Willers, K. Dai, J. Xu, Q. Zheng and M. Zheng, Inter J Biol Sci, 2011, 7, 968-977.

20. R. Pallela, S. Bojja and V. R. Janapala, Int J Biol Macromol, 2011, 49, 85-92.

21. D. W. Green, Biomed Mater, 2008, 3, 034010.

22. F. Nudelman, K. Pieterse, A. George, P. H. H. Bomans, H. Friedrich, L. J. Brylka, P. A. J. Hilbers, G. de With and N. A. J. M. Sommerdijk, Nat Mater, 2010, 9, 1004-1009.

23. D. J. DeMaster, Geophys Mono Ser, 1991, 63, 363-367.

24. M. P. G. Bostrom, K. J. Saleh and T. A. Einhorn, Orthop Clin North Am, 1999, 30, 647-658.

25. S. R. Thaller, A. Dart and H. Tesluk, Ann Plast Surg, 1993, 31, 429-433.

26. P. C. Bessa, M. Casal and R. L. Reis, J Tissue Eng Regen Med, 2008, 2, 81-96.

27. A. H. Reddi, J Cell Biochem, 1994, 56, 192-195.

28. A. H. Reddi, Nat Med, 1997, 3, 837-839.

29. J. M. Schmitt, K. Hwang, S. R. Winn and J. O. Hollinger, J Orthop Res, 1999, 17, 269-278.

30. J. A. Plumb, R. Milroy and S. B. Kaye, Cancer Res, 1989, 49, 4435-4440.

31. R. Zhukauskas, R. A. Dodds, C. Hartill, T. Arola, R. R. Cobb and C. Fox, Journal of Biomaterials Applications, 2010, 24, 639-656.

32. D. Gerlier and N. Thomasset, J Immunol Method, 1986, 94, 57-63.

33. Q. Lu, K. Ganesan, D. T. Simionescu and N. R. Vyavahare, Biomaterials, 2004, 25, 5227-5237.

34. L. M. Pineda, M. Busing, R. P. Meinig and S. Gogolewski, J Biomed Mater Res, 1996, 31, 385-394.

35. L. J. Gibson and M. F. Ashby, Cellular Solids: Structure and Properties, Cambridge University Press, London, 1999.

36. T. S. Karande, J. L. Ong and C. M. Agrawal, Ann Biomed Eng, 2004, 32, 1728-1743.

37. R. H. Li and J. M. Wozney, Trends Biotech, 2001, 19, 255-265.

38. V. Vogel and G. Baneyx, Annu Rev Biomed Eng, 2003, 5, 441-463.

39. J. P. Bilezikian, G. A. Rodan and L. G. Raisz, Principles of Bone Biology, Academic Press, San Diego, 2 edn., 2002.

40. N. Datta, H. L. Holtorf, V. I. Sikavitsas, J. A. Jansen and A. G. Mikos, Biomaterials, 2005, 26, 971-977.

41. A. E. Postlethwaite, J. M. Seyer and A. H. Kang, Proc Nat Acad Sci, 1978, 75, 871-875.

42. B. Fubini, G. Zanetti, S. Altilia, R. Tiozzo, D. Lison and U. Saffiotti, Chem Res Toxicol, 1999, 12, 737-745.

43. S. Kim, Y. Kang, C. A. Krueger, M. Sen, J. B. Holcomb, D. Chen, J. C. Wenke and Y. Yang, Acta Biomater, 2012, 8, 1768-1777.

44. T. L. Arinzeh, S. J. Peter, M. P. Archambault and C. Bos, J Bone Joint Surg Am, 2003, 85A, 1927-1935.

45. B. Kundu, S. K. Nandi, S. Dasgupta, S. Datta, P. Mukherjee, S. Roy, A. K. Singh, T. K. Mandal, P. Das, R. N. Bhattacharya and D. Basu, J Mater Sci: Mater Med, 2011, 22, 705-720.

46. S. K. Nandi, S. K. Ghosh, B. Kundu, D. K. De and D. Basu, Small Rumin Res, 2008, 75, 144-153.

47. R. Hou, F. Chen, Y. Yang, X. Cheng, Z. Gao, H. O. Yang, W. Wu and T. Mao, J Biomed Mater Res A, 2007, 80, 85-93.

48. C. J. Gibson, V. F. Thornton and W. A. Brown, Calcif Tissue Inter, 1978, 26, 29-31.

49. S. K. Nandi, B. Kundu, S. Datta, D. K. De and D. Basu, Res Vet Sci, 2009, 86, 162-173.

50. K. Tatsuyama, Y. Maezawa, H. Baba, Y. Imamura and M. Fukuda, Eur J Histochem, 2000, 44, 269-278.

51. C. Xiao, H. Zhou, S. Ge, T. Tang, H. Hou, M. Luo and X. Fan, Int J Mol Med, 2010, 26, 517-525.

52. K. V. Brown, B. Li, T. Guda, D. S. Perrien, S. A. Guelcher and J. C. Wenke, Tissue Eng A, 2011, 17, 1735-1746.

53. A. H. Reddi, Tissue Eng, 2000, 6, 351-359.

54. U. Ripamonti, J Cell Molecular Med, 2004, 8, 169-180.

55. U. Ripamonti, Biomaterials, 2006, 27, 807-822.

56. M. D. Schofer, P. P. Roessler, J. Schaefer, C. Theisen, S. Schlimme, J. T. Heverhagen, M. Voelker, R. Dersch, S. Agarwal, S. Fuchs-Winkelmann and J. R. Paletta, PLoS One, 2011, 6, e25462.

57. B. Levi, A. W. James, E. R. Nelson, D. Vistnes, B. Wu, M. Lee, A. Gupta and M. T. Longaker, PLoS One, 2010, 5, e11177.

58. M. C. Phipps, W. C. Clem, S. A. Catledge, Y. Xu, K. M. Hennessy, V. Thomas, M. J. Jablonsky, S. Chowdhury, A. V. Stanishevsky, Y. K. Vohra and S. L. Bellis, PLoS One, 2011, 6, e16813.

59. S. Ehnert, J. Baur, A. Schmitt, M. Neumaier, M. Lucke, S. Dooley, H. Vester, B. Wildemann, U. Stockle and A. K. Nussler, PLoS One, 2010, 5, e14073.

60. Z. S. Haidar, R. C. Hamdy and M. Tabrizian, Biotechnol Lett, 2009, 31, 1817-1824.

61. L. Meinel, E. Zoidis, J. Zapf, P. Hassa, M. O. Hottiger, J. A. Auer, R. Schneider, B. Gander, V. Luginbuehl and R. Bettschart-Wolfisberger, Bone, 2003, 33, 660-672.

62. J. R. Lieberman, A. Daluiski and T. A. Einhorn, J Bone Joint Surg, 2002, 84, 1032-1044.

63. S. R. Winn, H. Uludag and J. O. Hollinger, Adv Drug Deliv Rev, 1998, 31, 303-318.

64. D. H. R. Kempen, M. C. Kruyt, L. Lu, C. E. Wilson, A. V. Florschutz, L. B. Creemers, M. J. Yaszemski and W. J. A. Dhert, Tissue Eng Part A, 2008, 15, 587-594.

65. S. S. Kim, S. J. Gwak and B. S. Kim, J Biomed Mater Res A, 2008, 87, 245-253.

66. O. Jeon, S. J. Song, H. S. Yang, S.-H. Bhang, S.-W. Kang, M. Sung, J. H. Lee and B.-S. Kim, Biochem Biophys Res Commun, 2008, 369, 774-780.

Legends of table and figures:

Table 1: Score sheet prepared for different cellular events at 3 months after observing the histological images for all group of animals (N=3)

Table 2: Score sheet prepared for radiological assessment of bone formation for different implants up to 3 months (N=3)

Fig. 1: Glimpse of SEM of bioscaffold converted from marine sponge (*Biemna fortis*) to actual sample (both inset)

Fig. 2: DTA-TGA thermogram of freeze-dried marine sponge up to 1000^{o} C in air atmosphere

Fig. 3: XRD of (a) as received freeze-dried, (b) 725^{o} C and (c) 1190^{o} C fired powders

Fig. 4: FTIR spectra of (a) as received freeze-dried, (b) 725^{o} C and (c) 1190^{o} C fired powders

Fig. 5: (a) Monolayer culture of MC3T3 cells and (b) formazan crystals formed after adding MTT in treated cell culture of MC3T3

Fig. 6: SEM of the powders fired at 725^{o} C

Fig. 7: SEM of the porous scaffold prepared at 1190^{o} C

Fig. 8: In vitro release kinetics of IGF-1 and BMP-2 in vitro in α-MEM upto 28 days (inset: cumulative pattern profile)

Fig. 9: SEM of the defect site of in vivo bone sample (a) and (b) without any implant, (c) and (d) with bare porous scaffold (1190^{o} C), (e) and (f) with porous scaffold loaded with IGF and (g) and (h) BMP after 3 months

Fig. 10: Histology of bone section taken after 3 months with (a) no implant, (b) bare porous scaffold, (c) porous scaffold loaded with IGF and (d) BMP-2

Fig. 11: Fluorochrome labeling of bone taken after 3 months with (a) no implant, (b) bare porous scaffold, (c) porous scaffold loaded with IGF and (d) BMP-2 (1. golden yellow fluorescence represents new bone and 2. sea green appearance depicts old bone)

Fig. 12: Radiographs taken after day '0', 1, 2 and 3 months post-operatively for (a) no implant, (b) bare porous scaffold, (c) porous scaffold loaded with IGF and (d) BMP-2

Table 1: Score sheet prepared for different cellular events at 3 months after observing the histological images for all group of animals (N=3)

Parameter	**Control group**	**Bare converted sponge scaffold**	**Scaffold with BMP-2**	**Scaffold with IGF-1**
Fibro-vascular proliferation	1.3	1^{a}	1.7	2^{a}
Infiltration with mononuclear cells	1. 3	1.7	1.7	2
Osteoclastic activity	1^{b}	1.7	2.3^{b}	2.7^{b}
Mucin deposit	0.7	0.7	1	1.3
Vascularity	1^{c}	1.7	2.3^{c}	2.7^{c}
Osteoblastic activity	1.3^{d}	2	2.3	2.7^{d}

(0) Absence, (1) mild, (2) moderate, (3) marked, (4) severe

Superscripts a-d denote $p \leq 0.05$ for that said set of groups

Table 2: Score sheet prepared for radiological assessment of bone formation for different implants up to 3 months (N=3)

Implant	**0 Day**	**1 Month**	**2 Month**	**3 Month**
Control	0	1	1	2
Bare sponge scaffold	0	1	2	3
IGF-1 impregnated sponge scaffold	0	2	3	4
BMP-2 impregnated sponge scaffold	0	2	3	4

0 - No bone formation in defect

1 - Bone just extending into the defect

2 - Bone substantially bridging the cortical defect

3 - Bone fully bridging the cortex without significant callus

4 - Bone fully bridging the cortex with distinct overlying callus

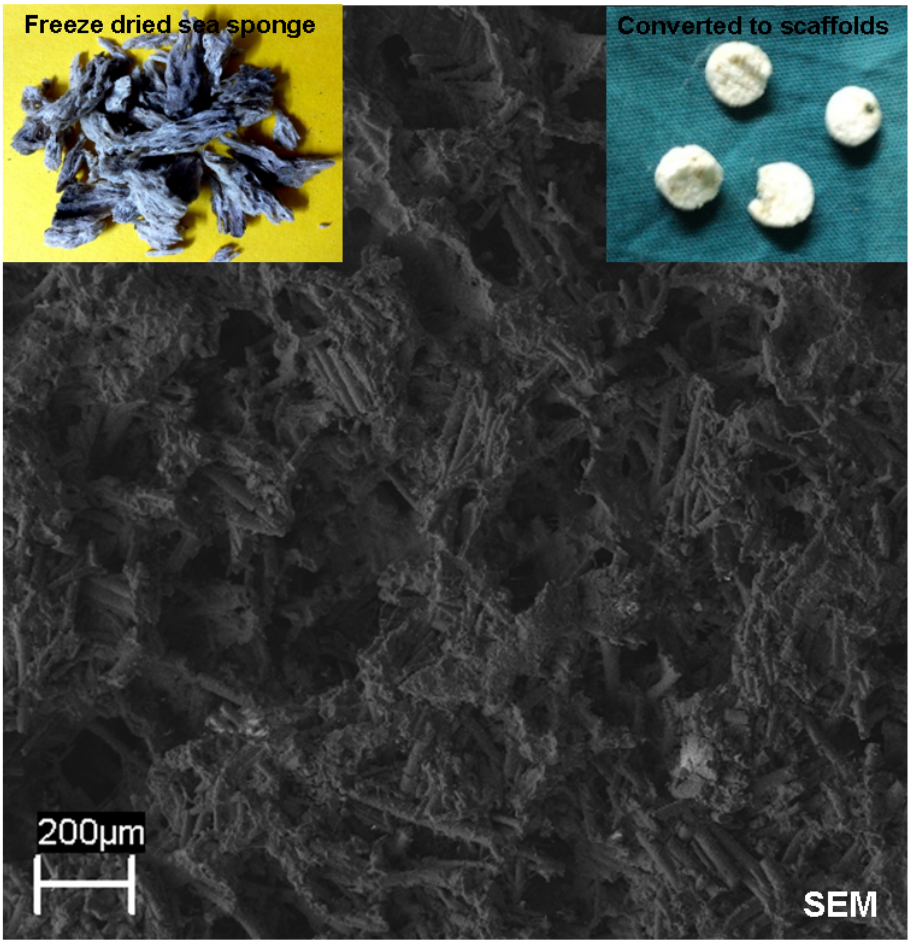

Fig. 1: Glimpse of SEM of bioscaffold converted from marine sponge (Biemna fortis) to actual sample (both inset) 134x137mm (150 x 150 DPI)

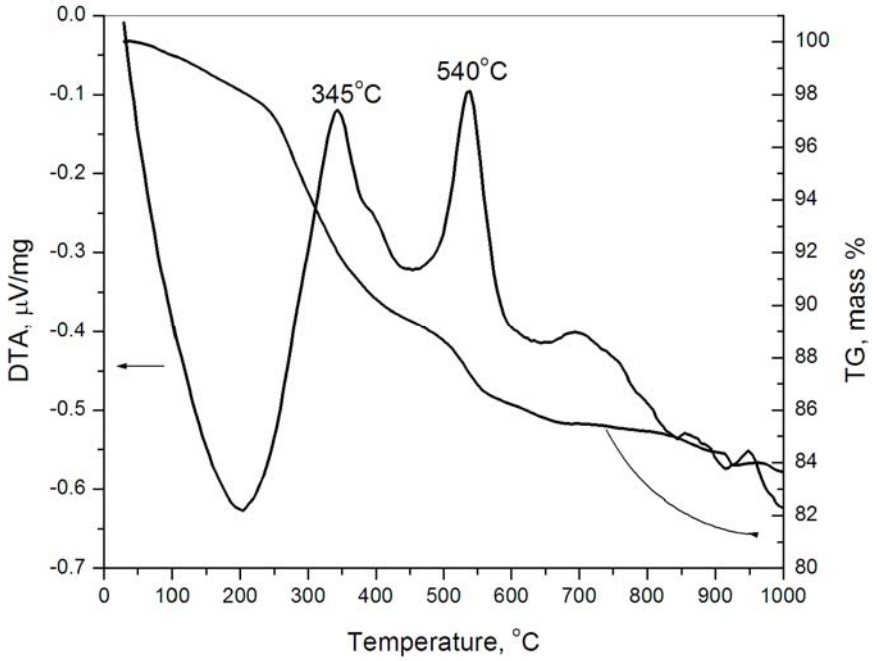

Fig. 2: DTA-TGA thermogram of freeze-dried marine sponge up to 1000 oC in air atmosphere 279x215mm (150 x 150 DPI)

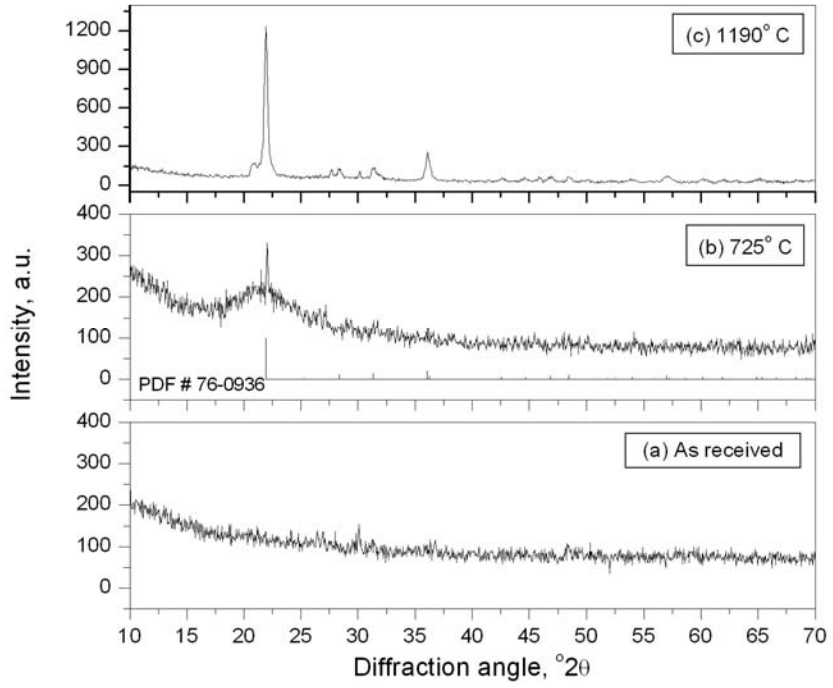

Fig. 3: XRD of (a) as received freeze-dried, (b) 725 oC and (c) 1190 oC fired powders 279x215mm (150 x 150 DPI)

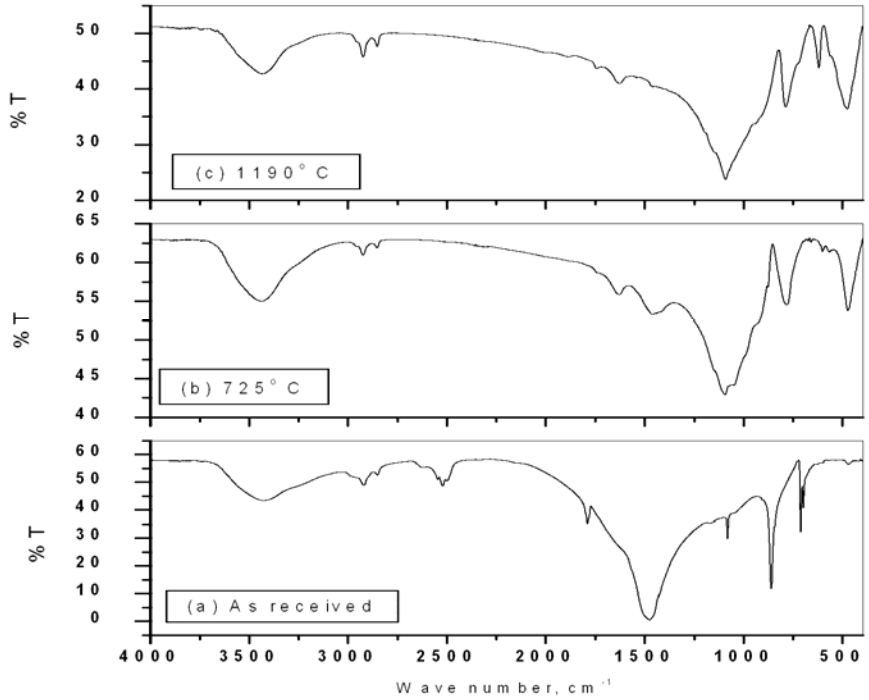

Fig. 4: FTIR spectra of (a) as received freeze-dried, (b) 725 oC and (c) 1190 oC fired powders 279x215mm (150 x 150 DPI)

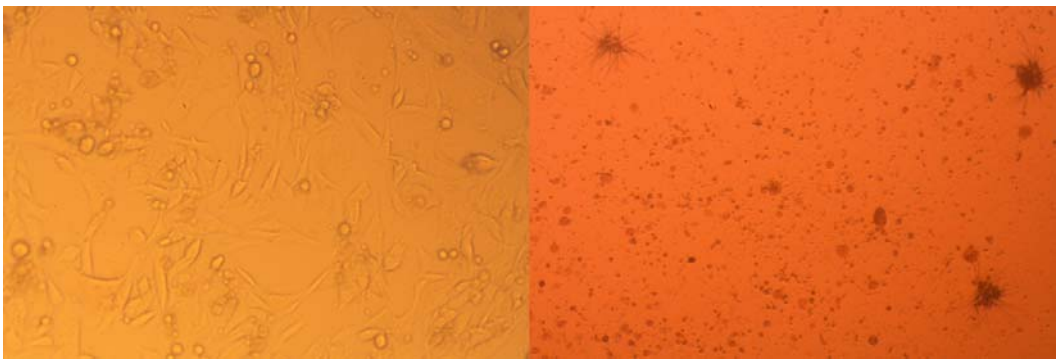

Fig. 5: (a) Monolayer culture of MC3T3 cells and (b) formazan crystals formed after adding MTT in treated cell culture of MC3T3 379x126mm (150 x 150 DPI)

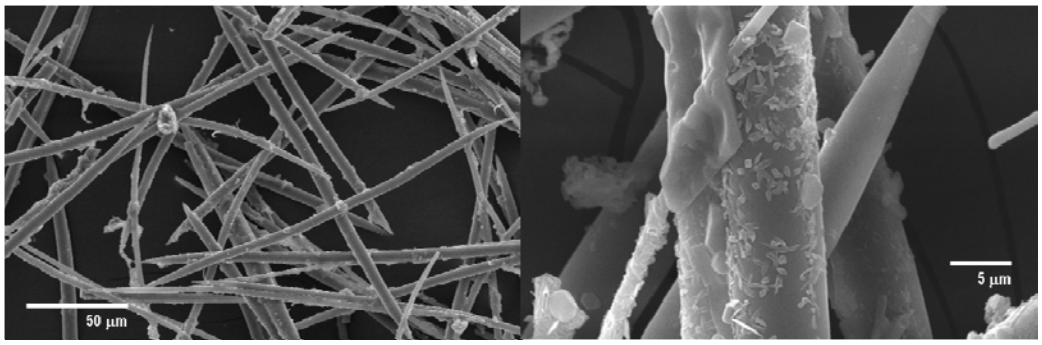

Fig. 6: SEM of the powders fired at 725 oC 256x82mm (150 x 150 DPI)

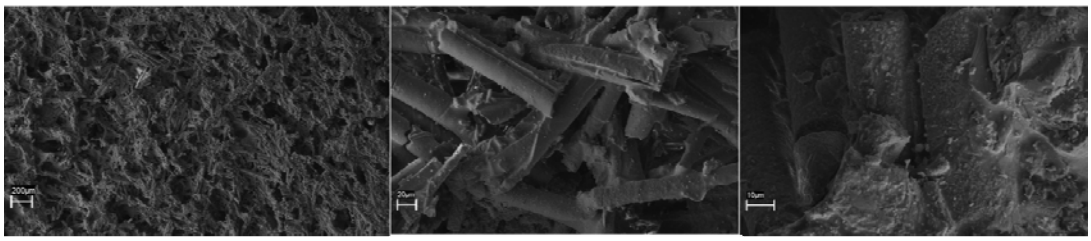

Fig. 7: SEM of the porous scaffold prepared at 1190 oC 300x64mm (150 x 150 DPI)

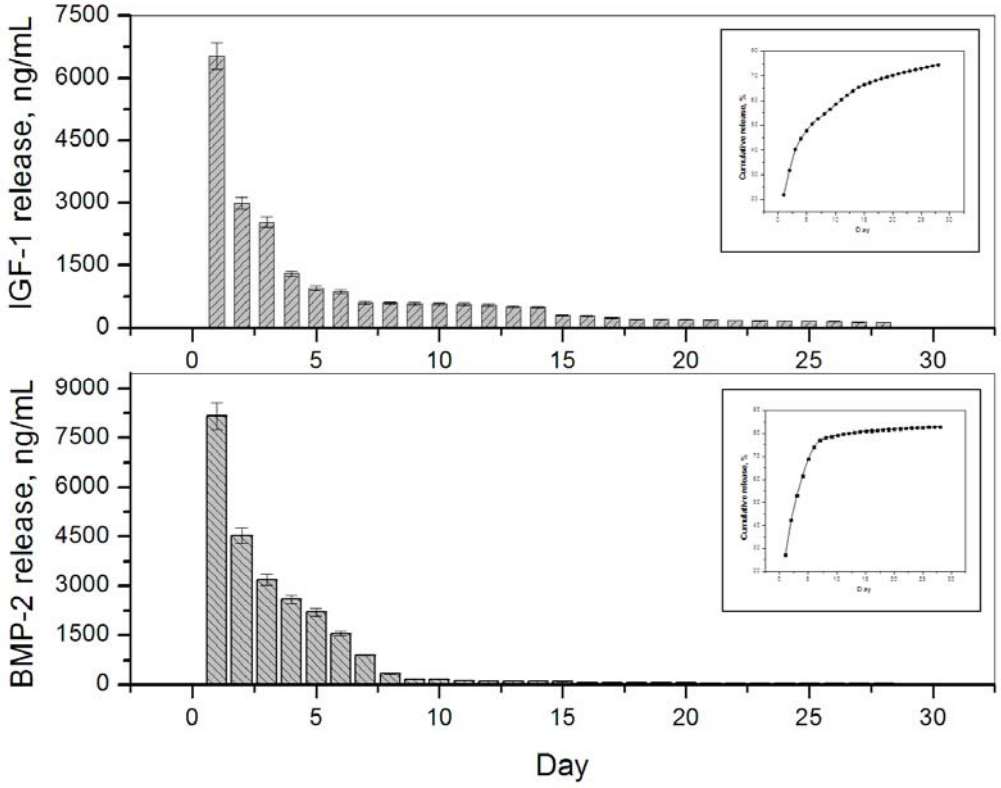

Fig. 8: In vitro release kinetics of IGF-1 and BMP-2 in vitro in α-MEM upto 28 days (inset: cumulative pattern profile) 279x215mm (150 x 150 DPI)

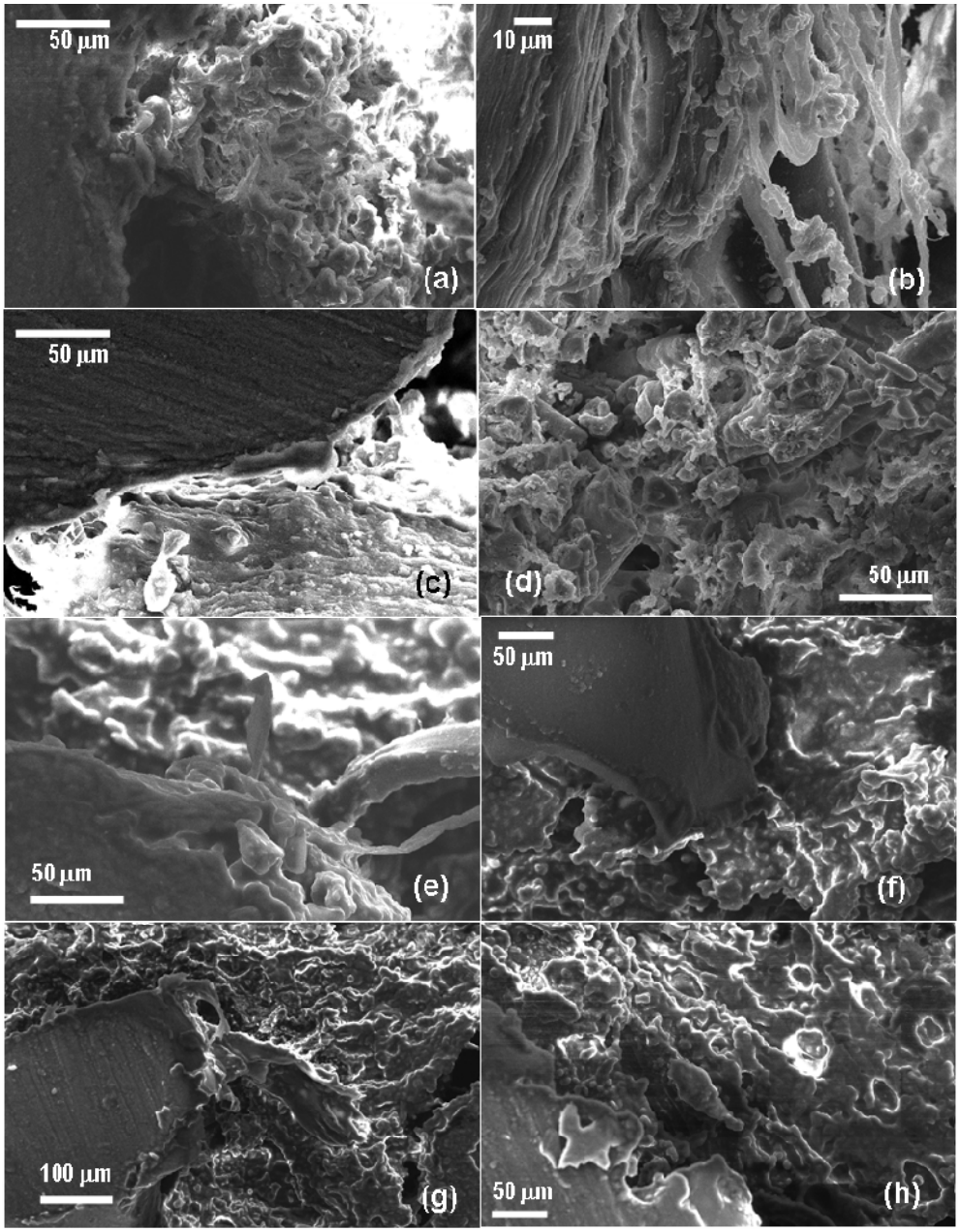

Fig. 9: SEM of the defect site of in vivo bone sample (a) and (b) without any implant, (c) and (d) with bare porous scaffold (1190 oC), (e) and (f) with porous scaffold loaded with IGF and (g) and (h) BMP after 3 months 136x175mm (150 x 150 DPI)

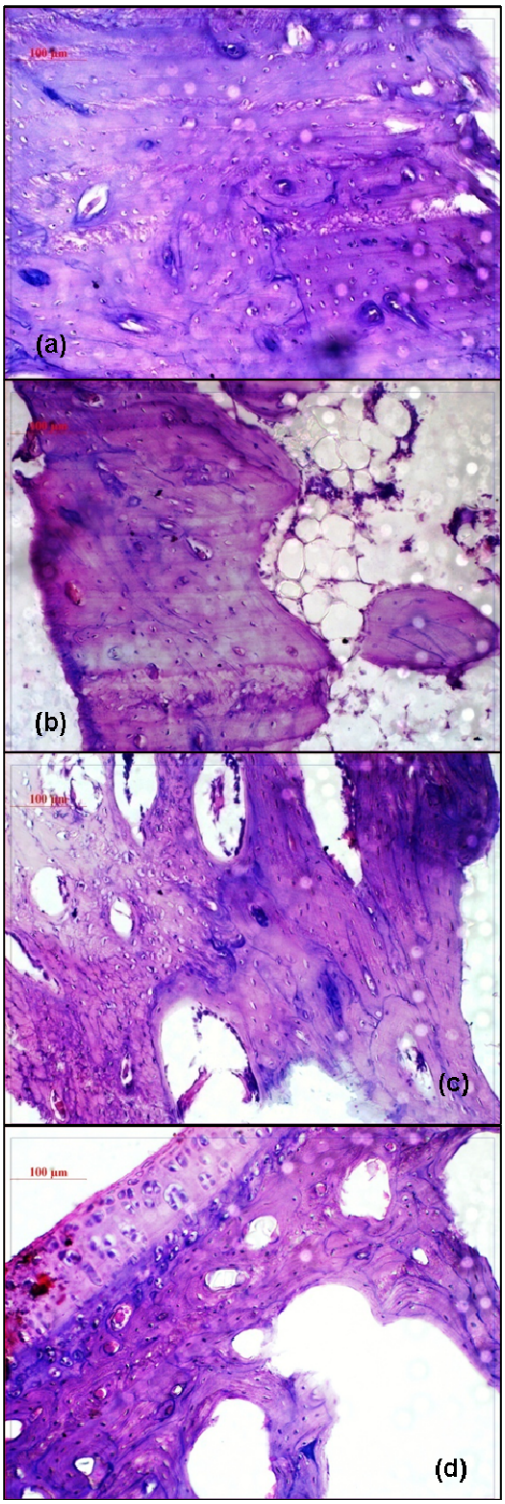

Fig. 10: Histology of bone section taken after 3 months with (a) no implant, (b) bare porous scaffold, (c) porous scaffold loaded with IGF and (d) BMP-2 81x245mm (150 x 150 DPI)

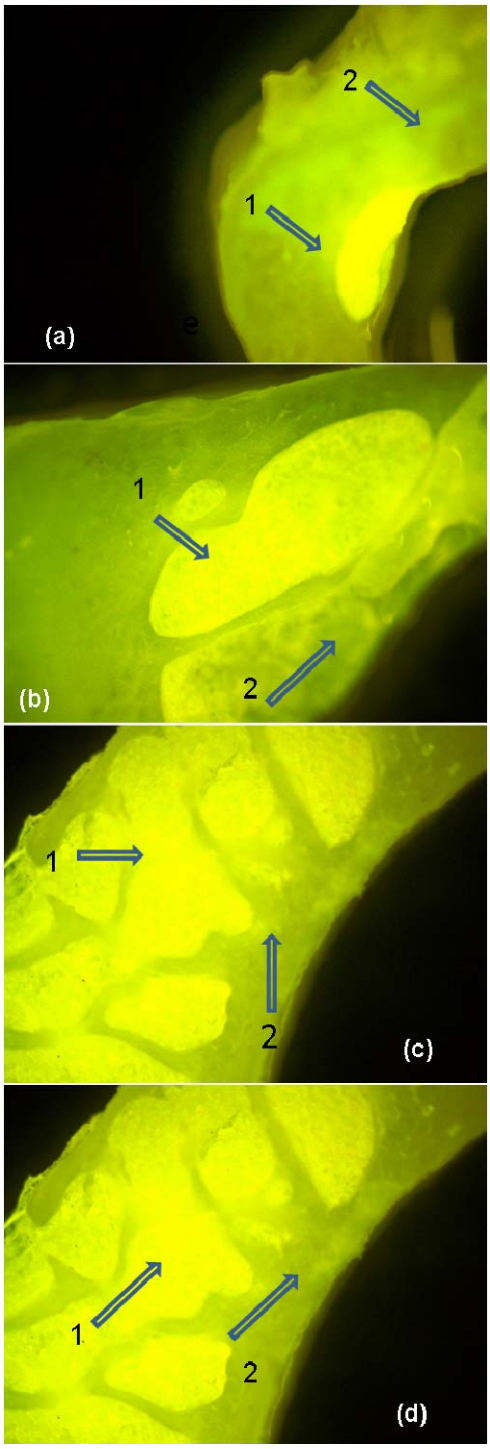

Fig. 11: Fluorochrome labeling of bone taken after 3 months with (a) no implant, (b) bare porous scaffold, (c) porous scaffold loaded with IGF and (d) BMP-2 (1. golden yellow fluorescence represents new bone and 2. sea green appearance depicts old bone) 82x245mm (150 x 150 DPI)

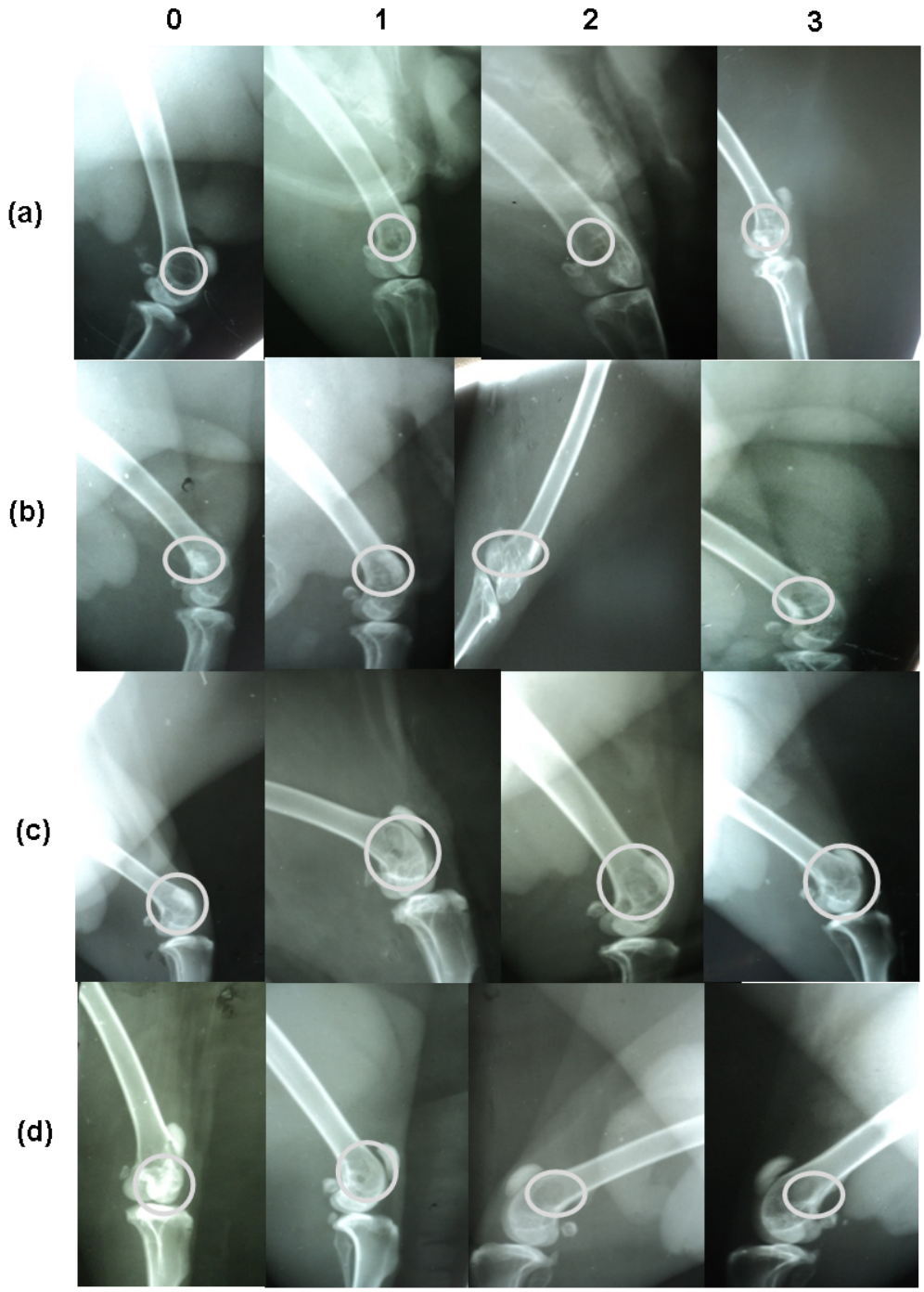

Fig. 12: Radiographs taken after day '0', 1, 2 and 3 months post-operatively for (a) no implant, (b) bare porous scaffold, (c) porous scaffold loaded with IGF and (d) BMP-2 144x194mm (150 x 150 DPI)